Materials Today Bio 23 (2023) 100859

Contents lists available at ScienceDirect

Materials Today Bio

journal homepage: www.journals.elsevier.com/materials-today-bio

OpiCa1-PEG-PLGA nanomicelles antagonize acute heart failure induced by the cocktail of epinephrine and caffeine

Jun Li [a,b,1], Fei Wang [b,1], Xinyan Liu [c,1], Zhixiao Yang [b,f], Xiaoyu Hua [b], Hongqiao Zhu [c], Carmen R. Valdivia [d], Li Xiao [d,e], Songyu Gao [b], Héctor H. Valdivia [d,***], Liang Xiao [b,**], Jinming Wang [a,*]

[a] College of Veterinary Medicine, Shanxi Agricultural University, ShanXi, TaiGu, 030801, China
[b] Department of Occupational and Environmental Health, Faculty of Naval Medicine, Naval Medical University (Second Military Medical University), Shanghai, 200433, China
[c] Department of Traditional Chinese Medicine Surgery, The First Affiliated Hospital of the Navy Medical University (Changhai Hospital), Shanghai, 200433, China
[d] Department of Medicine and Cardiovascular Research Center, University of Wisconsin-Madison School of Medicine and Public Health, Madison, WI, USA
[e] Department of Forensic Toxicological Analysis, West China School of Basic Medical Sciences & Forensic Medicine, Sichuan University, Chengdu, 610065, China
[f] Teaching and Research Department of Chinese Pharmacy, Yunnan Traditional Chinese Medicine, YunNan, KunMing, 650500, China

ARTICLE INFO

Keywords:
OpiCa1-PEG-PLGA nanomicelle
Acute heart failure
β-adrenergic stress
RyR_2
Ca^{2+}

ABSTRACT

Background: Reducing Ca^{2+} content in the sarcoplasmic reticulum (SR) through ryanodine receptors (RyRs) by calcin is a potential intervention strategy for the SR Ca^{2+} overload triggered by β-adrenergic stress in acute heart diseases.

Methods: OpiCal-PEG-PLGA nanomicelles were prepared by thin film dispersion, of which the antagonistic effects were observed using an acute heart failure model induced by epinephrine and caffeine in mice. In addition, cardiac targeting, self-stability as well as biotoxicity were determined.

Results: The synthesized OpiCa1-PEG-PLGA nanomicelles were elliptical with a particle size of 72.26 nm, a PDI value of 0.3, and a molecular weight of 10.39 kDa. The nanomicelles showed a significant antagonistic effect with 100 % survival rate to the death induced by epinephrine and caffeine, which was supported by echocardiography with significantly recovered heart rate, ejection fraction and left ventricular fractional shortening rate. The FITC labeled nanomicelles had a strong membrance penetrating capacity within 2 h and cardiac targeting within 12 h that was further confirmed by immunohistochemistry with a self-prepared OpiCa1 polyclonal antibody. Meanwhile, the nanomicelles can keep better stability and dispersibility *in vitro* at 4 °C rather than 20 °C or 37 °C, while maintain a low but stable plasma OpiCa1 concentration *in vivo* within 72 h. Finally, no obvious biotoxicities were observed by CCK-8, flow cytometry, H&E staining and blood biochemical examinations.

Conclusion: Our study also provide a novel nanodelivery pathway for targeting RyRs and antagonizing the SR Ca^{2+} disordered heart diseases by actively releasing SR Ca^{2+} through RyRs with calcin.

1. Introduction

In common heart diseases such as heart failure, myocardial infraction, and certain arrhythmias e.g. catecholamine polymorphic ventricular tachycardia (CPVT), the elevated Sarcoplasmic reticulum (SR) Ca^{2+} under β1 adrenergic stimulation by sympathetic excitation acompanied with abnormal Cardiac ryanodine receptor (RyR2) functions by mutation, or the changes of phosphorylation, nitration or

* Corresponding author.
** Corresponding author.
*** Corresponding author.
E-mail addresses: lijun6459@hotmail.com (J. Li), feiwang116@163.com (F. Wang), 13816390825@139.com (X. Liu), 13609846821@163.com (Z. Yang), huaxiaoyu0828@163.com (X. Hua), 529564126@qq.com (H. Zhu), crvaldivia@medicine.wisc.edu (C.R. Valdivia), xiao52@wisc.edu (L. Xiao), songyu3012014@outlook.com (S. Gao), hhvaldiv@medicine.wisc.edu (H.H. Valdivia), hormat830713@hotmail.com (L. Xiao), jm50408@163.com (J. Wang).
[1] These authors contributed equally to this work.

https://doi.org/10.1016/j.mtbio.2023.100859
Received 26 August 2023; Received in revised form 17 October 2023; Accepted 7 November 2023
Available online 8 November 2023

binding proteins e.g. Calmodulin antibody (CaM) and FKBP12.6 (synchronously cause the increase of diastolic SR Ca^{2+} leakage and the decrease of SR Ca^{2+} release threshold, which generally leads to the increase of cytosolic Ca^{2+} and delayed depolarization (DAD) through Na^{+}-Ca^{2+} exchanger (NCX) on the cell membrane, triggering abnormal action potential and a series of ventricular tachyarrhythmias such as premature ventricular contraction (PVC), ventricular tachycardia (VT), ventricular fibrillation (VF), and even cardiac death [1–6]. Due to the various causes of pathological factors and forms of functional abnormalities in RyR2, compared to restoring its functional state, preventing excessive SR Ca^{2+} elevation is a relatively simple and uniform strategy for antagonizing Ca^{2+} disordered damages under β1 adrenergic stimulation in heart diseases [7,8].

In addition to the two strategies of directly inhibiting sympathetic excitation by using β1 receptor blockers and reducing SR Ca^{2+} reuptake by inhibiting phospholamben (PLN) phosphorylation and the overactivation of the Ca^{2+}-ATPase SERCA, we used a novel kind of RyR targeting peptide ligand calcin to partially activate RyR2, so as to increase its open frequency and actively release the SR Ca^{2+}, which is also a potential strategy to prevent excessive SR Ca^{2+} elevation, and the feasibility of this strategy was confirmed on CPVT by using a representative Imperacalcin (also named as Imperatoxin A) in our previous studies [9–15]. Nevetheless, as a spherical peptide containing 33–35 amino acids, calcin has been found to mainly antagonize gentle PVCs or non-sustained BVTs rather than severe sustained BVTs or PVTs; like most of peptide drugs, calcin was also found to have a fast metabolic rate *in vivo*, of which the half-life is even less than 2 h, therefore, it is necessary to improve its drug efficacy by increasing the local concentration in heart, as well as to extend its action duration by controlled release through pharmaceutic methods [16,17].

Methoxy poly(ethylene glycol)-Poly(L-lactide-*co*-glycolide) (PEG-PLGA) is one of the most commonly used biodegradable amphiphilic block copolymers (ABCs) for drug delivery applications [18–23], where PLGA forms the hydrophobic core and can be used for encapsulation and controlled release of hydrophobic drugs, while the outer circumference is hydrophilic PEG, which can improve the stability of nanomicelles and carry hydrophilic drugs through its carboxyl group [24,25]. Moreover, the nanomicelles can be controllably degraded into the small coumponds e.g. lactic acid and glycolic acid from PLGA, ethylene glycol and diethylene glycol from PEG, respectively, all of which can enter the citric acid cycle for further utilization without any toxic side effects [21,22,26–28]. Therefore, PEG-PLGA nanomicelle is an ideal drug carrier for enhancing calcin's antagonistic effect on Ca^{2+} disordered damages under β adrenergic stress [29,30].

In this study, the Opicalcin-PEG-PLGA (OpiCa1-PEG-PLGA) nanomicelles were firstly synthesized by the connection between the most active member of the calcin family, Opicalcin1 (OpiCa1) and the PEG-PLGA polymer, of which the antagonistic effects were then observed on the lethal acute heart failure induced by the cocktail of epinephrine and caffeine in mice. Further researches were conducted on cardiac targeting, self-stability as well as biotoxicity of nanomicelles, so as to provide a basis for the development of a calcin-derived nanodelivery system against the SR Ca^{2+} overload related heart diseases.

2. Materials and methods

2.1. Synthesis and screening of OpiCa1-PEG-PLGA nanomicelles

2.1.1. Synthesis

10 mg –COOH–mPEG-b-PLGA was dissolved in 1 mL phosphate buffer to obtain a solution concentration of 10 mg/mL 0.4 g of 1-(3-Dimethylaminopropyl)-3-ethylcarbodiimide hydrochloride (EDC) and 0.6 g of N-Hydroxysuccinimide (NHS) was added to the above solution. The reaction was continued for 2 h to activate the carboxyl terminus of –COOH–PEG-PLGA [31]. Dialysis was performed three times in 1 × PBS for 4 h each. Then 10 mg/mL OpiCa1 was added in activation of –COOH–PEG-PLGA at a concentration of 10 mg/mL. Stirred for 2 h at RT. An appropriate amount of the OpiCa1-PEG-PLGA nanomicelle solution was dissolved in organic solvent and dried at 55 °C. Then dissolved in deionized water at 60 °C, and filtered through 0.22 μm microporous filter membrane to obtain the OpiCa1-PEG-PLGA nanomicelle solution [32].

2.1.2. Screening

OpiCa1-PEG-PLGA nanomicelles were prepared by thin film dispersion method and dialysis method in four organic solvents dimethyl sulfoxide (DMSO), methanol (MeOH), dichloromethane (DCM) and isopropyl alcohol (IPA) respectively. Then the particle size, Zeta potential and PDI of each preparation were detected to investigate the optimal preparation conditions of nanomicelles. *Film dispersion method*: 10 mg PEG-PLGA finished product was precisely weighed and poured into a glass dish containing 1 mL of DMSO, MeOH, DCM and IPA respectively. It was completely dissolved by blowing with a pipetting gun, and evaporated in a vacuum chamber at 60 °C to form a uniform film. The prepared 60 °C deionized water was sucked with a 1 mL pipetted gun, the formed film was dissolved, and then sucked out into a 15 mL centrifuge tube, which could be repeatedly sucked for three times, vortexed for 1 min, centrifuged at 1000 × *g* for 5 min, and filtered by 0.22 μm microporous filter membrane to obtain OpiCa1-PEG-PLGA nanomicelle solution [33]. *Dialysis method*: The finished product of 10 mg –COOH–PEG-PLGA was precisely weighed and poured into an organic solvent glass dish containing 1 mL DMSO, MeOH, DCM and IPA. It was completely dissolved by blowing with a pipetting gun, the solution was introduced into a dialysis bag (MW 3500) and placed into a beaker containing 2 L of 1 × PBS for dialysis. Dialysis was performed three times in 1 × PBS for 4 h each, and filtered through 0.22 μm microporous filter membrane to obtain the OpiCa1-PEG-PLGA nanomicelle solution [34].

2.2. Opimization and charaterization

The particle size, Zeta potential and PDI were measured by Malvern laser particle size analyzer (Zetasizer nano ZS, UK). The characteristic functional groups, molecular weight shifts and structural deformation were detected by infrared spectroscopy (FT-IR, MEXUS, USA), Raman spectroscopy (Renishaw, in Via, UK), gel permeation chromatography (GPC, 1260 Infinity II, UK) and X-ray diffraction (XRD, Kratos, Japan). The morphological structure of the sample was observed by transmission electron microscope (TEM, JEOL-1230, Japan).

2.3. Survival of ICR mice

ICR mice 5–8 weeks old were obtained from Shanghai (CN). These mice were mixed and divided into control, Caff and Epi, PEG-PLGA, OpiCal and OpiCal-PEG-PLGA group. The survival rates were recorded by inserting four subcutaneous needle electrodes into the subcutaneous tissue of the limbs (PowerLab system, ADInstruments) while the anesthetized mice were placed on a heating pad with a rectal temperature of 36.8 °C–37.2 °C. Caff (120 mg/kg) and Epi (2 mg/kg) and were injected intraperitoneally to induce ventricular tachyarrhythmias 5 min and were monitored continuously for 30 min. Then PEG-PLGA, OpiCal (5 mg/kg), and OpiCal-PEG-PLGA (containing OpiCal 5 mg/kg) were pre-injected via the tail vein after Epi and Caff injection to observe their antagonistic effect on survival rate in mice (n = 6).

2.4. Ultrasonic cardiogram

ICR mice were divided into control, Caff and Epi, OpiCa1, PEG-PLGA and OpiCa1-PEG-PLGA groups (n = 6). The OpiCa1 (5 mg/kg), PEG-PLGA and OpiCa1-PEG-PLGA nanomicelles (containing OpiCa1 5 mg/kg) were injected intravenously in sequence respectively after Caff (120 mg/kg) and Epi (2 mg/kg) were injected intraperitoneally in each group

10 min except control. After 60 min, the transparent gel was gently placed the chest of the mice so that the probe could transmit ultrasound. The heart rate (HR), cardiac ejection fraction (EF), and left ventricular fractional shortening rate (FS) were detected for cardiac function analysis by Small Animal Ultrasound Imaging System (Vevo 2100, USA).

2.5. Cell culture and membrane penetrating effect

H9C2 cells, an adherent cell line derived from BD1X rat embryonic heart tissue, were grown in DMEM medium with high glucose containing 10 % fetal bovine serum and 1 % antibiotics, cultured at 37 °C, 5 % CO_2 and saturated humidity. A number of 5000 cells per well were seeded in confocal culture dishes and cultured until in logarithmic growth phase. After the replacement of old medium by 1 mL serum-free medium, 2 mL OpiCa1 or OpiCa1-PEG-PLGA nanomicelles containing 100 μM OpiCa1 was added to each dish. The transmembrane effiency of OpiCa1 and OpiCa1-PEG-PLGA namomicelles was observed under a fluorescence microscope (Zeiss LSM 710, Germany) at 0, 30, 60 and 120 min.

2.6. Immunohistochemistry

The paraffin sections were placed in a 60 °C oven for 30–60 min, then placed in xylene I, II, III for 10 min each, 100 %, 95 %, 80 %, 70 % ethanol gradient for 2 min each, and washed with water for 5 min. PBS was washed 3 times for 3 min each time. The sections were then infiltrated with preheated blocking permeabilization solution (40 mL PBS, 120 μL TritonX-100, 400 μL 30 % H_2O_2) for 30 min (in the dark at RT) and washed three times with PBS for 3 min each time. Some nonspecific binding sites were then blocked with serum from the same source as the secondary antibody, and the primary antibody was incubated overnight at 4 °C. PBS was washed 3 times for 3 min each time. The secondary antibodies were incubated at 37 °C for 2 h and washed three times with PBS for 3 min each. After 10 min of color development with DAB-H_2O_2, color development was terminated with distilled water. Image J 1.51 software was used for fluorescence intensity.

2.7. Living imaging

ICR mice 5–8 weeks old were mixed and divided into control, PEG-PLGA, OpiCa1 and OpiCa1-PEG-PLGA group (n = 6). *In vivo* imaging was performed at 12 h after intravenous injection of PEG-PLGA, OpiCa1 and OpiCa1-PEG-PLGA nanomicelles. The IVIS Spectrum small animal *in vivo* imaging system (IVScope 8000, USA) was used to monitor the distribution of nanomicelles.

2.8. Stability test

Stability of in Vitro: Firstly, 5 mL of OpiCa1-PEG-PLGA nanomicelles were prefrozen at −20 °C and −80 °C for 12 h respectively. The powder was put into a freeze dryer and dried at −55 °C for 24 h under reduced pressure to obtain the OpiCa1-PEG-PLGA lyophilized powder. The particle size, Zeta potential and PDI of OpiCa1-PEG-PLGA was measured at 0, 4, 8, 12, 24, 48 and 72 h respectively [35,36]. ***Stability of in vivo*:** The OpiCa1-PEG-PLGA lyophilized powder was obtained by the same method as described above. It was finely weighed and suspended in 3 mL medium containing 10 % fetal bovine serum, and incubated at 37 °C for 72 h to simulate the physiological environment. The particle size of OpiCa1-PEG-PLGA was measured at 0, 4, 8, 12, 24, 48 and 72 h respectively, to observe the effect of serum on the stability of OpiCa1-PEG-PLGA nanomicelles [37].

2.9. Plasma concentration

Blood samples were collected from mice at 0.05, 0.25, 1, 2, 4, 6, 24, 48 and 72 h before and after injection of 5 mg/kg OpiCa1 (OpiCa1 antibody prepared by Global genetics), 3000 × *g* for 15 min to obtain serum. Sera were mixed 1:100 with coating buffer in 96-well plates and incubated coated at 4 °C, washed three times with PBST for 15 min each, and blocked with 1 % BSA (bovine serum albumin) PBST for 1 h at room temperature. Primary rabbit serum antibody was diluted 1:80 and incubated for 1 h at RT and washed 3 times with PBST for 15 min each time. The secondary goat anti-rabbit IgG-HRP was then incubated at 1:500 dilution for 1 h at RT. Bound antibodies were detected at 450 nm by TMB solution.

2.10. Flow cytometry

The H9C2 cells were cultured by conventional methods. The cells were spread in 6-well plates and 2 mL culture medium was added after 24 h. The culture medium was discarded, and the OpiCa1-PEG-PLGA (OpiCal was 100 μM) was added to the final volume of 2 mL per well. The cells were cultured in an incubator with 5 % CO_2 for 12 h at 37 °C. Cells were resuspended in 400 μL of 1 × Annexin V binding solution at a concentration of approximately 1×10^6 cells/mL. A total of 100 μL (1×10^6 cells/mL) of the cell suspension was aspirated into a 5 mL culture tube, and 5 μL of Annexin V-FITC and 5 μL of Propdium lodide staining solution were added. After vortexing the cells gently, the cells were incubated at RT (25 °C) in the dark for 15 min. An additional 400 μL of binding buffer was added to each well to collect all cells after blowing and passing through the membrane, and the fluorescence intensity was measured by flow cytometry (BD FACS Calibur, USA).

2.11. CCK-8

H9C2 cardiomyocytes were grown in DMEM medium containing 10 % fetal bovine serum and 1 % antibiotics, cultured at 37 °C, 5 % CO_2. The above cells were seeded in 96-well plates (5000 per well). Then the PEG-PLGA, OpiCa1 and OpiCa1-PEG-PLGA were coated with 20, 30, 40, 50, 60, 80 and 100 μM respectively (n = 6). After 12 h of incubation, 10 μL CCK-8 solution (10 % in DMEM) was added to each well and incubated in the incubator for 45 min. Cell viability was calculated by measuring absorbance at 450 nm by microplate reader (Varioskan LUX, USA).

2.12. Hematological and pathological tests

ICR mice were intravenously injected with control, OpiCa1, PEG-PLGA and OpiCa1-PEG-PLGA (containing OpiCa1 5 mg/kg, n = 6) for 12 h. Blood was drawn from the inner canthus of the eyes and placed in an anticoagulant centrifuge tube to detect alanine aminotransferase (ALT) and aspartate aminotransferase (AST). Creatine kinase (CK), creatine kinase isoenzyme (CK-MB), lactate dehydrogenase (LDH), creatinine (Cr) and uric acid (UA) were taken out. The specimens were fixed with 4 % fixed paraformaldehyde universal tissue fixative and subjected to routine hematoxylin-eosin (HE) staining for histopathological examination by Shanghai Bolf Biological Company.

2.13. Statistics

All results were expressed as X ± SD. GraphPad Prism 8.0.2 software was used for statistical analysis. Statistical significance was calculated using the two-tailed non-parametric Mann-Whitney T test for two groups' comparison. *P < 0.05; **P < 0.01.

3. Results

3.1. Synthesis and screening

The OpiCa1-PEG-PLGA polymers were firstly synthesized through an amide crosslink between the amino group of OpiCa1 and the carboxyl group of PEG-PLGA in the presence of the two activators EDC and NHS

which was to dissolve in different organic solvents, including DMSO, MeOH, DCM and IPA, to form fat-soluble films, and then use surfactant deionized water to disperse them into the water phase to spontaneously form nanomicelles which were composed of OpiCa1 polypeptide molecules as the shell, and the PLGA end of PEG-PLGA as the core to form an elliptical spherical structure [38–40]. (Fig. 1A). A total of eight OpiCa1-PEG-PLGA nanomicelles were self-asembled with two methods in four different organic sovents, and their particle size, Zeta potential and polydispersity index (PDI) were determined under the same conditions (Fig. 1B∼1G). In the dialysis method, the particle size and Zeta potential of the nanomicelles generated in the four solutions DMSO, MeOH, DCM and IPA were very close, approximately 200 nm and −14 mV, respectively. In contrast, the PDI value in DMSO was around 0.15, significantly smaller than that in other three solutions with the values between 0.6–0.9. In the thin film dispersion method, a significant difference was that the nanoparticle size in IPA was 68.29 ± 3.28 nm, which was far smaller than that in other three solutions between 200–300 nm. The mean values of Zeta potential in IPA and DCM exceeded −25, which was much larger than those in MeOH and DMSO with the values of −16.80 ± 0.73 and −7.52 ± 0.51 respectively, and indicated a better stability. The PDI values in four solutions were between 0.6–1.0, where the value in DMSO was the smallest while in IPA was the largest [41–44]. In summary, although the dispersibility of the OpiCa1-PEG-PLGA nanomicelles by thin film dispersion method in IPA needed further improvement, it had the smallest particle size and the best stability, making it a candidate nanoparticle for further research.

3.2. Opitimization and characterization

The candidate OpiCa1-PEG-PLGA nanomicelles by film dispersion in IPA were further optimized by ultrasound, follwed by systematically characterization with a series of methods such as TEM, DLS, FT-IR,

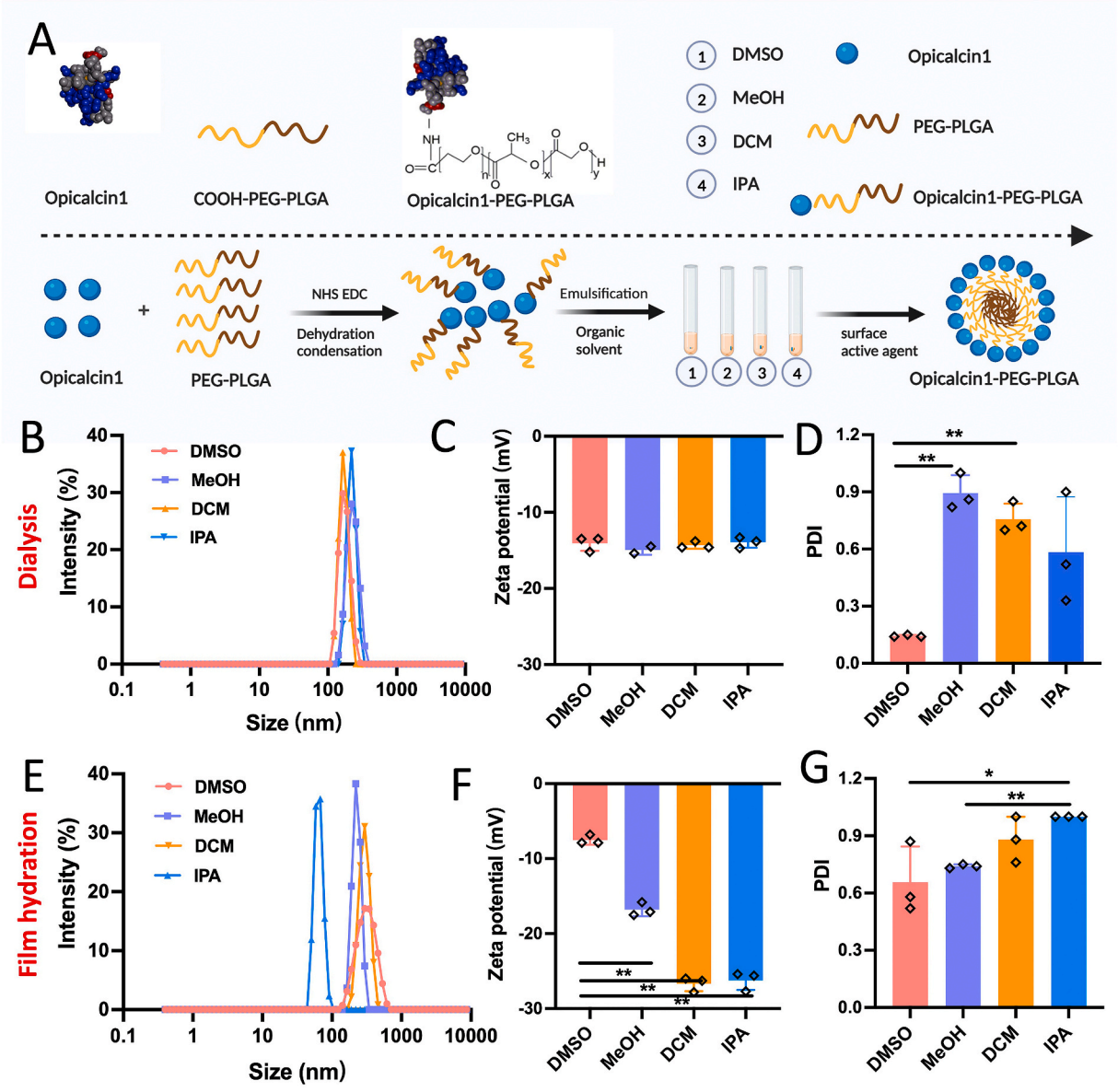

Fig. 1. Synthesis and screening of OpiCa1-PEG-PLGA nanomicelles. (**A**) The schematic representation of OpiCa1-PEG-PLGA nanomicelles in different organic solvents. (**B**) Size distribution of OpiCa1-PEG-PLGA by dialysis method, (**C**) Zeta potential and (D) PDI of OpiCa1-PEG-PLGAin DMSO, MeOH, DCM, and IPA by dialysis method; (**E**) Size distribution of OpiCa1-PEG-PLGA by thin film hydration; (**F**) Zeta potential and (**G**) PDI of OpiCa1-PEG-PLGA nanomicelles in DMSO, MeOH, DCM and IPA by film hydration; (Mean ± SD, n = 3). Statistical significance was calculated using the two-tailed non-parametric Mann-Whitney T test for two groups' comparison. *P < 0.05; **P < 0.01.

Raman, XRD and GPC. Both of the nanomicelles PEG-PLGA and OpiCa1-PEG-PLGA displayed elliptical shapes by TEM (Fig. 2A), where the OpiCa1-PEG-PLGA was slightly larger in particle size than that of the blank PEG-PLGA (Fig. 2B). In contrast, the Zeta

potential of the OpiCa1-PEG-PLGA was higher than that of the PEG-PLGA (Fig. 2C), and the PDI values were both around 0.3, which were greatly improved and indicated a good disperivity of OpiCa1-PEG-PLGA after the opimization by ultrasound (Fig. 2D). FT-IR found that all three samples had two segements 500~1750 cm^{-1} and 2750~3750 cm^{-1} with similar peak distributions and shapes, and the obvious difference comes from the complete disapperance of a very narrow and sharp peak at around 2600 cm^{-1} in PEG-PLGA after connecting with OpiCa1 (Fig. 2E) [29,45]. There were also two peak segments >2500 cm^{-1} and 500~2000 cm^{-1} observed by Raman spectroscopy, among which the shapes were similar in the segement >2500 cm^{-1} whereas the peak distributions and shapes between 500 and 2000 cm^{-1} seemed disorderly [46,47]. In addition, OpiCa1-PEG-PLGA showed an iconic sharp peak between 1250 and 1500 cm^{-1} and two peaks among 500~1250 cm^{-1} disappeared in PEG-PLGA (Fig. 2F). The biggest difference tested by XRD was the disappearance of the narrow and sharp peak between 11.90–11.98° in PEG-PLGA after the connection (Fig. 2G) [48]. Finally, the molecular weight (MW) of OpiCa1-PEG-PLGA was around 10.39 kDa by GPC that is roughly the sum of OpiCa1′ MW of 3.88 kDa and PEG-PLGA's MW of approximate 7.00 kDa (Fig. 2H). All of the results indicated that OpiCa1-PEG-PLGA nanomicelles was successfully synthesized by the connection OpiCa1 and PEG-PLGA.

3.3. Efficiency

Mouse survival analysis and echocardiography were used to evaluate the effect of OpiCa1-PEG-PLGA nanomicelles on lethal acute heart failure induced by the cocktail of caffeine (Caff) and epinephrine (Epi) in mice. When we administered 120 mg/kg Caff and 2 mg/kg Epi intravenously to ICR mice, it was found that all mice died within 30 min. The intervention of PEG-PLGA had no effect, and its death time was completely the same as that of the control group. But when we injected 5 mg/kg OpiCa1 and OpiCa1-PEG-PLGA equivalent to 5 mg/kg OpiCa1, the survival rates of both were significantly improved where OpiCa1-PEG-PLGA achieved a 100 % survival rate, and OpiCa1 exceeded 80 %, indicating that OpiCa1 and its OpiCa1-PEG-PLGA nanomicelle had a significant antagonistic effect on Epi and Caff induced lethal acute heart failure (Fig. 3A). The results of similar antagonistic effects were also confirmed in echocardiography (Fig. 3B). The heart rates (HRs) of mice decreased from 400 bpm to less than 100 bpm after injection of Caff and Epi cocktail, and PEG-PLGA did not show any effect. Both OpiCa1 and OpiCa1-PEG-PLGA significantly recovered to a heart rate close to that of

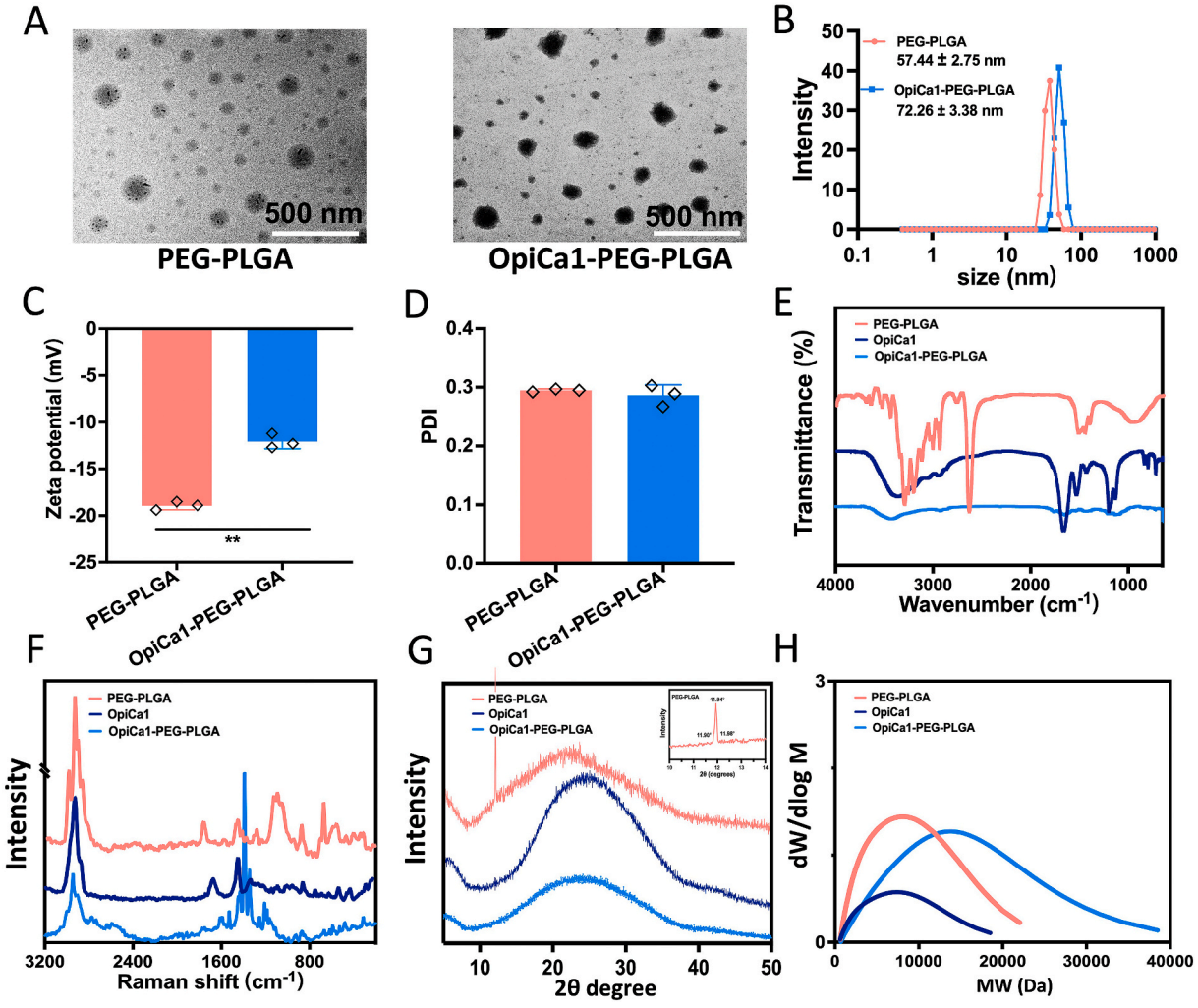

Fig. 2. TEM images of **(A)** PEG-PLGA micelles and OpiCa1-PEG-PLGA nanomicelles; **(B)** The particle size distribution of PEG-PLGA and OpiCa1-PEG-PLGA nanomicelles (Mean ± SD, n = 3); **(C)** The Zeta Potential, **(D)** PDI, **(E)** FT-IR, **(F)** Raman spectra, **(G)** X-ray diffraction and (H) GPC of PEG-PLGA, OpiCa1 and OpiCa1-PEG-PLGA nanomicelle. Statistical significance was calculated using the two-tailed non-parametric Mann-Whitney T test for two groups' comparison. *P < 0.05; **P < 0.01.

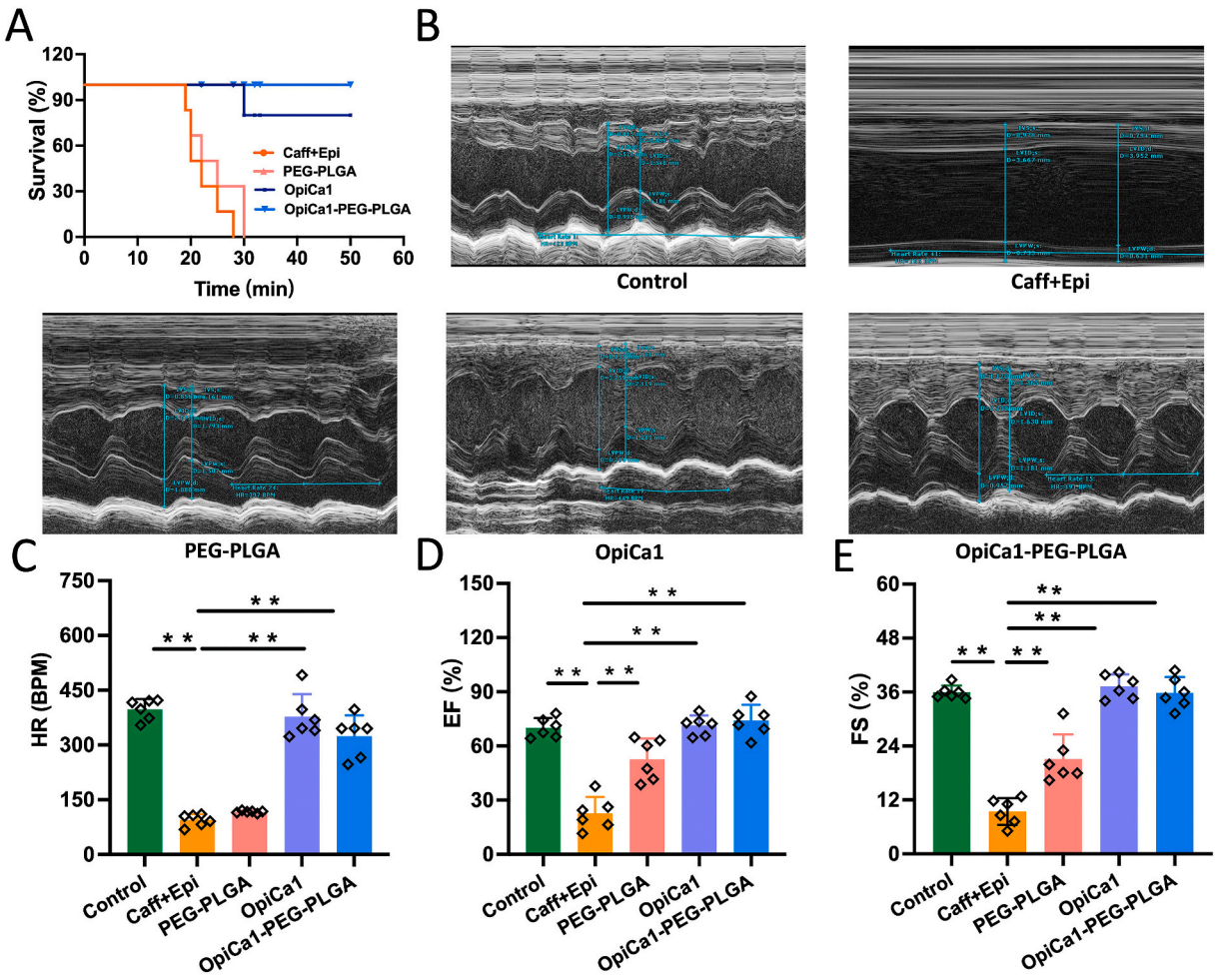

Fig. 3. The evaluation of OpiCa1-PEG-PLGA nanomicelles for sudden cardiac death induced by adrenaline and caffeine in mice. (A) The survival of mice were injected with OpiCa1 (5 mg/kg), PEG-PLGA (5 mg/kg) and OpiCa1-PEG-PLGA (5 mg/kg) nanomicelles after Caff (120 mg/kg) and Epi (2 mg/kg) administration; **(B)** The echocardiography of mice in control, Caff + Epi, PEG-PLGA, OpiCa1 and OpiCa1-PEG-PLGA. **(C)** The heart rate, **(D)** EF, **(E)** FS statistics of mice were injected with OpiCa1 and OpiCa1-PEG-PLGA nanomicelles 10 min after Caff (120 mg/kg) and Epi (2 mg/kg) administration through Echocardiography (Mean ± SD, n = 6). Statistical significance was calculated using the two-tailed non-parametric Mann-Whitney T test for two groups' comparison. *P < 0.05; **P < 0.01.

the control group (Fig. 3C). Similar results also appeared in the ejection fraction (EF) (Fig. 3D) and left ventricular fractional shortening rate (FS) (Fig. 3 E) indicators, which showed that OpiCa1 and OpiCa1-PEG-PLGA were completely restored to normal, and PEG-PLGA had a gentle trend of partial recovery [49,50]. In all, The results from survival rate and echocardiography indicated that OpiCa1-PEG-PLGA nanoparticles retain the activity of OpiCa1 and have the effect of antagonizing the lethal acute heart failure induced by Caff and Epi.

3.4. Targeting

Membrane penetrating effect and cardiac targeting of OpiCa1 and OpiCa1-PEG-PLGA nanomicelles were compared and explored at the levels of myocardial cells and intact animals. By using H9C2 cells and FITC labeled OpiCa1 and OpiCa1-PEG-PLGA nanomicelles, we found that both could penetrate the cell membrane and enter myocardial cells within 120 min. However, the difference between the two was that FITC labeled OpiCa1 penetrated the cell membrane with a faster initial rate with the first hour, while the rate of FITC labeled OpiCa1-PEG-PLGA nanomicelles entering the cells was significantly accelerating within 2h, indicating that OpiCa1 has the ability to carry PEG-PLGA polymers into myocardial cells (Fig. 4Ã~4D). At the same time, compared to the scattered distribution of FITC labeled PEG-PLGA, both FITC labeled OpiCa1 and OpiCa1-PEG-PLGA nanomicelles were more concentrated in cardiac tissues within 12 h, thereby exhibiting good cardiac targeting *in vivo* (Fig. 4E and F and Fig. S2). Finally, we used the method of immunohistochemistry with self-prepared OpiCa1 polyclonal antibody and found that both OpiCa1 and OpiCa1-PEG-PLGA nanomicelles were significantly distributed in cardiac tissue, further confirming the cardiac targeting of OpiCa1 and OpiCa1-PEG-PLGA nanomicelles (Fig. 4G and H).

3.5. Stability

The stability of OpiCa1-PEG-PLGA nanomicelles mainly includes the change of particle parameters in PBS solution, OpiCa1 cocentration in 10 % serum and plasama *in vitro*, as well as the change of plasma OpiCa1 concentration *in vivo*. In PBS solution, there were no significant changes in parameters including particle size, Zeta potential, and PDI at 4 °C within 72 h for both the control PEG-PLGA and OpiCa1-PEG-PLGA nanomicelles. However, at 20 °C and 37 °C, both of the nanomicelles showed a significant increase in particle size, with 37 °C increasing more than 20 °C. In contrast, the temperature showed a similar upward effect on Zeta potential in OpiCa1-PEG-PLGA nanomicelles but little in the control. Conversely, the temperature had significant influence on PDI in the control instead of OpiCa1-PEG-PLGA nanomicelles (Fig. 5Ã~5F). Overall, the OpiCa1-PEG-PLGA nanomicelles kept stable under 4 °C PBS conditions within 3 days that can be used for short-term storage. In 10 %

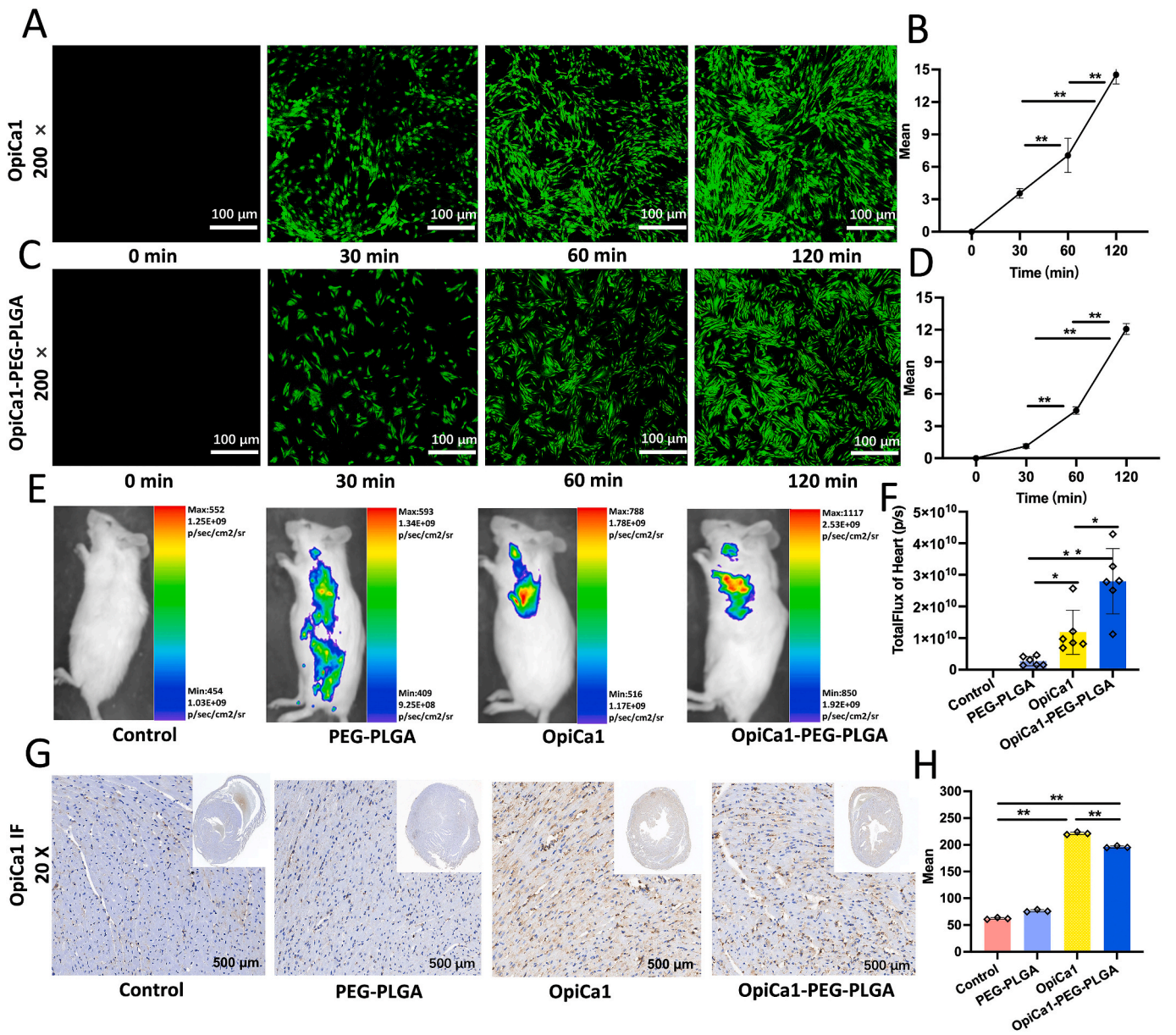

Fig. 4. Targeting of OpiCa1-PEG-PLGA nanomicelles. (A) The cell membrane penetration images of OpiCa1 and **(C)** OpiCa1-PEG-PLGA at 0, 30, 60 and 120 min; **(B)** The statistical analysis of fluorescence of OpiCa1 and **(D)** OpiCa1-PEG-PLGA at 0, 30, 60 and 120 min; **(E)** The living image and **(F)** The total heart fluorescence intensity statistics of control, PEG-PLGA, OpiCa1 and OpiCa1-PEG-PLGA nanomicelles at 12 h in mice; **(G)** Cardiac immunohistochemistry and **(H)** The statistical analysis of immunohistochemistry of control, PEG-PLGA, OpiCa1 and OpiCa1-PEG-PLGA nanomicelles at 12 h (Mean ± SD, n = 6). Statistical significance was calculated using the two-tailed non-parametric Mann-Whitney T test for two groups' comparison. *P < 0.05; **P < 0.01).

serum, the concentration of free OpiCa1 increased within 72 h at 20 °C and 37 °C by ELISA with self-prepared OpiCa1 polyclonal antibody, while there was no obvious change at 4 °C (Fig. 5G). No significant increase in free OpiCa1 was observed in plasma at all temperatures within 72 h (Fig. 5H), indicating a more stablity in plasma than that in PBS solution and diluted serum. When free OpiCa1 was injected, it decreased with a very fast rate in the first 2–4 h, and completed disappeared within 48 h. In contrast, after injection of OpiCa1-PEG-PLGA nanoparticles, the initial concentration of free OpiCa1 was far lower than that of free OpiCa1 injection, and the plasma OpiCa1 concentration remained stable for 72 h, indicating that the OpiCa1-PEG-PLGA nanomicelles have a good sustained-release effect *in vivo* (Fig. 5I) there by maintaining the plasma OpiCa1 concentration for a longer period *in vivo*.

3.6. Biotoxicity

Finally, the biotoxicity of OpiCa1-PEG-PLGA nanomicelles was tested by flow cytometry and CCK8 for *in vitro* cytotoxicity, biochemical and pathological examinations for *in vivo* toxicity (Fig. 6 and Fig. S1). Among them, PEG-PLGA, OpiCa1, and OpiCa1-PEG-PLGA all showed very slight proapoptotic effects within 12 h, with a proportion of apoptotic cells of only about 1.5 % (Fig. 6A and B and Fig. S3), which was consistent with the results of CCK8 detection where the cell viabilities of all samples remained >90 % after 12 h of exposure at the concentrations up to 100 μM OpiCa1, indicating that the cytotoxicities of both OpCa1 and its derived OpiCa1-PEG-PLGA nanomicelles were very low (Fig. 6C) [51,52]. Similarly, there were no significant differences in cardiac function (CK, CK-MB, and LDH) (Fig. 6D), liver function (ALT and AST) (Fig. 6E), and renal function (Crea and UA) (Fig. 6F) among all samples after 12 h of treatment. Pathological examination

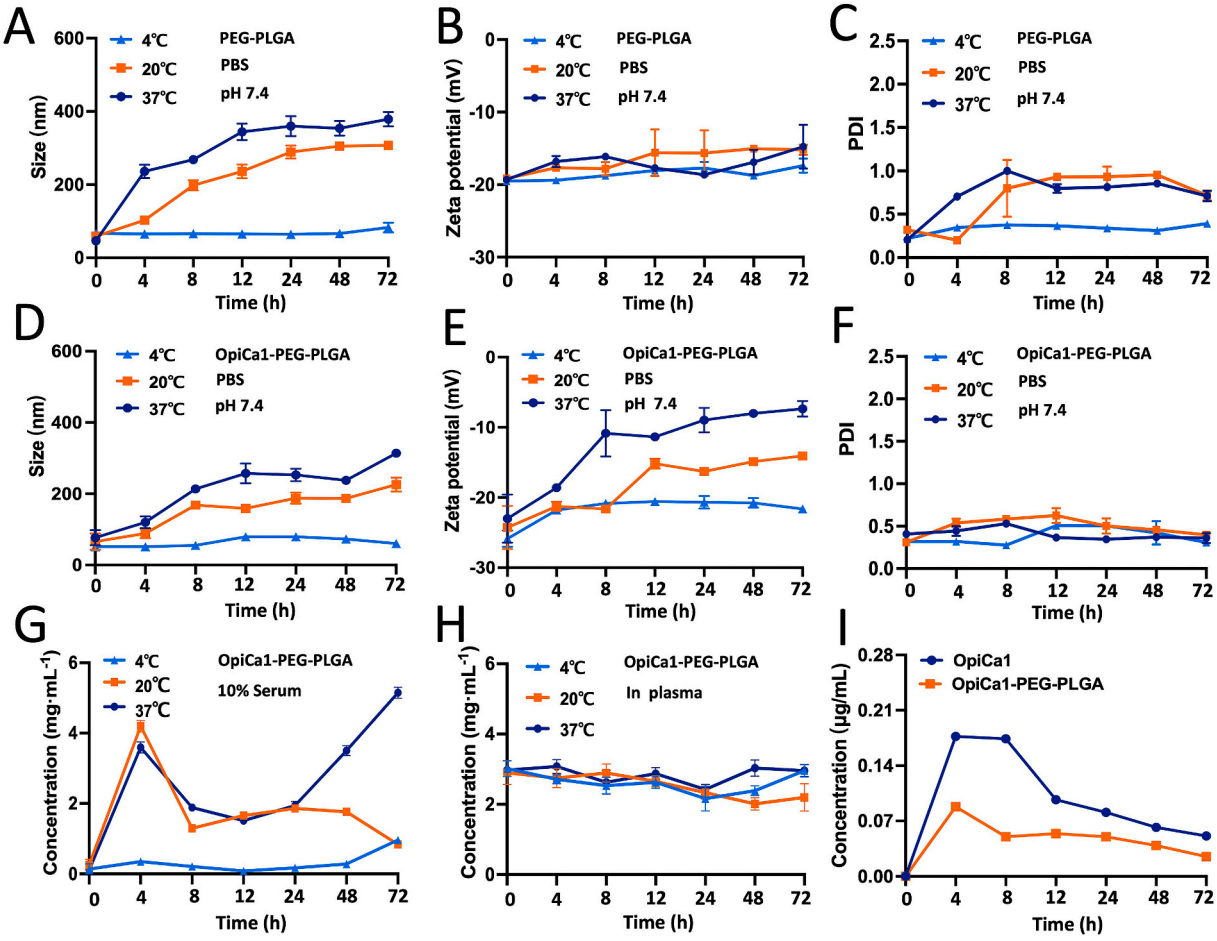

Fig. 5. Stability of the OpiCa1-PEG-PLGA nanomicelles. (A) The Size, **(B)** PDI and **(C)** Zeta potential of PEG-PLGA nanomicelles at 0, 4, 8, 12, 24, 48 and 72 h in PBS solution (pH 7.4) at 4 °C, 20 °C and 37 °C **(D)** The Size, **(E)** PDI and **(F)** Zeta potential of OpiCa1-PEG-PLGA nanomicelles at 0, 4, 8, 12, 24, 48 and 72 h in PBS solution (pH 7.4) at 4 °C, 20 °C and 37 °C (Mean ± SD, n = 6). **(G)** The concentration of OpiCa1-PEG-PLGA nanomicelles in 10 % serum. **(H)** The plasma concentration of OpiCa1-PEG-PLGA nanomicelles *in vitro*. **(I)** The plasma concentration of OpiCa1-PEG-PLGA nanomicelles *in vivo*. Statistical significance was calculated using the two-tailed non-parametric Mann-Whitney T test for two groups' comparison. *P < 0.05; **P < 0.01.

also obtained the same results, showing that all samples had clear myocardial fibers and stripes (Fig. 6G) with no *in vivo* toxicity [53].

4. Discussion

Calcin is a group of membrane penetrating peptides scorpion toxins that specifically target RyRs. It contains 33–35 amino acids and structurally is a globular molecule maintained by an ICK motif core that is folded by three pairs of disulfides [54,55]. On the spherical surface, all basic amino acids (≈30 %) aggregate on one side, while neutral and acidic amino acids are distributed on the other side, making it a typical class of spherical amphiphilic molecules. This special structure and charge distribution endow calcin with the ability to penetrate the cell membrane and specifically bind to RyRs, causing partial opening of RyRs by long-lasting subconductance and actively releasing Ca^{2+} from the SR [56,57]. Based on this characteristic, our previous research found that calcin only partially depletes the SR Ca^{2+}, with a maximum release ratio of approximate 60 %, therby preventing excessive elevation of SR Ca^{2+} under β adrenergic stress while maintaining normal cardiac excitation-contraction coupling and diastolic function under normal conditions [58,59]. By using the representatve calcin, Imperacalcin, we confirmed this hypothesis and found that it can antagonize SR Ca^{2+} overload related tachyarrhythmias such as PVCs and non-sustained BVTs in CPVT [55,60].

However, our previous research also found that its antagonistic effects were mainly concentrated in gender Ca^{2+} disordered ventricular tachyarrhythmias such as PVCs and non-sustained BVTs, and thus its antagonistic efficacy needs to be strengthened. On the other hand, as a peptide ligand of RyRs, calcin also has the common peptide characteristics of fast metabolism rate and relatively short efficacy time [61,62]. Therefore, extending the residence time in the body through a sustained-release effect is also an key question for calcin to enhance the antagonistic effect on heart diseases. Regarding this, OpiCa1-PEG-PLGA nanomicelles were synthesized in this study based on the most common non-toxic nanocarrier PEG-PLGA polymer [63–65]. We found that OpiCa1-PEG-PLGA nanomicelles keep almost the same effect as OpiCa1 in antagonizing the lethal acute heart failure induced by epinephrine and caffine, and exhibit good cardiac targeting, self-stability, as well as low toxicity. Especially, it was found that OpiCa1-PEG-PLGA nanomicelles maintain relatively stable long-term low concentrations of OpiCa1 in the body. Due to the high affinity between OpiCa1 and RyRs (~0.3 nM), a very small amount of OpiCa1 can achieve the prevention of SR Ca^{2+} increase under β adrenergic stress [11]. It can be seen that OpiCa1-PEG-PLGA micelles undoubtedly achieved the aim of sustained release of OpiCa1 and prolonging the OpiCa1 efficacy. Moreover, This study also provide a novel nanodelivery pathway for targeting RyRs and antagonizing the SR Ca^{2+} diordered heart diseases by actively releasing SR Ca^{2+} through partially increasing the open frequency of RyRs with calcin.

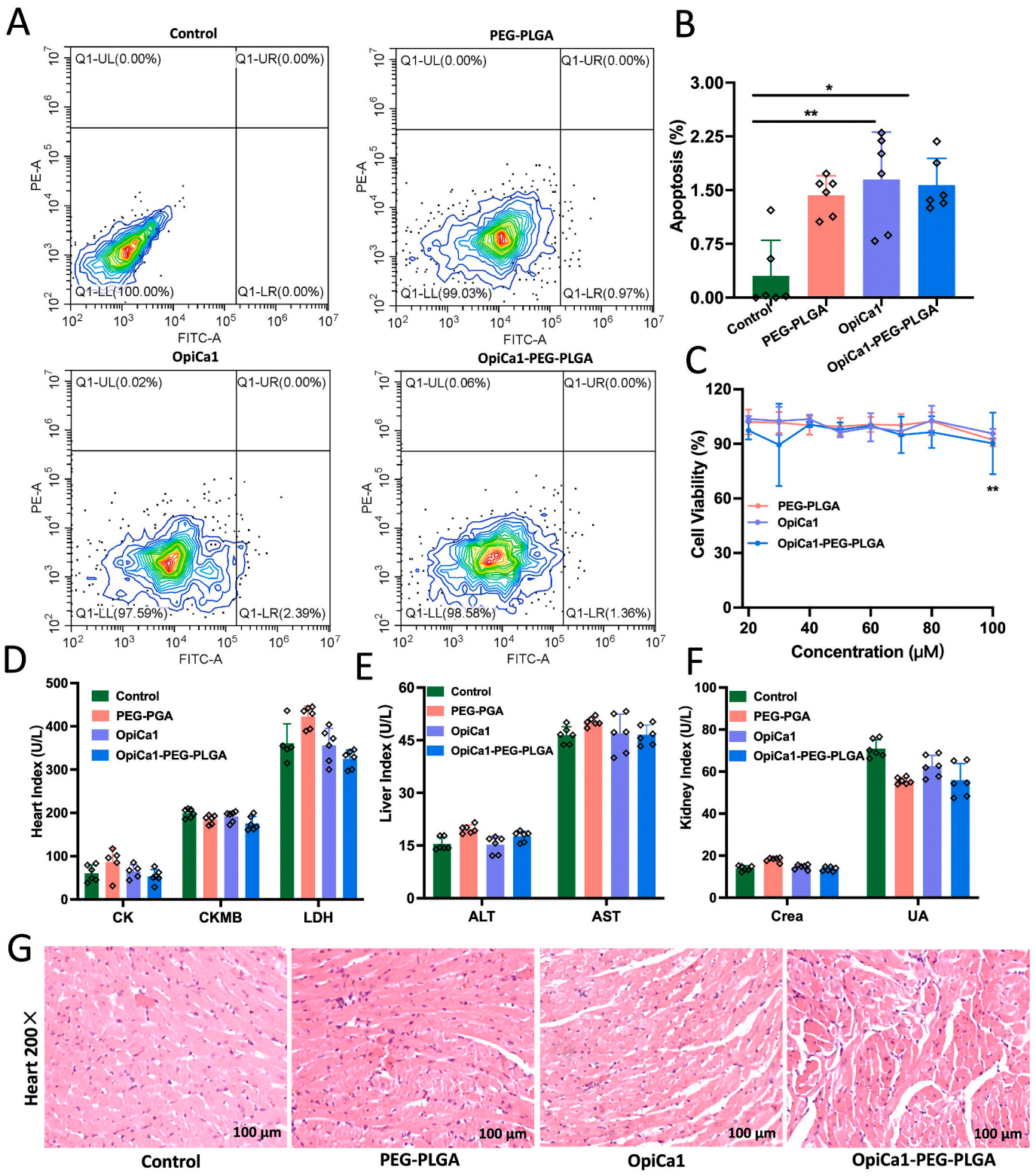

Fig. 6. The apoptosis of **(A)** Control, PEG-PLGA, OpiCa1 and OpiCa1-PEG-PLGA nanomicelles at 12 h; **(B)** The statistics of Control, PEG-PLGA, OpiCa1 and OpiCa1-PEG-PLGA nanomicelles at 12 h; **(C)** The cell viability of PEG-PLGA, OpiCa1 and OpiCa1-PEG-PLGA incubated at 20, 30, 40, 50, 60, 70, 80 and 100 μM for 12 h; **(D)** Heart index, **(E)** Liver index and **(F)** Kidney index of Control, PEG-PLGA, OpiCa1-PEG-PLGA nanomicelles. **(G)** H&E staining analysis of Heart of Control, PEG-PLGA, OpiCa1, and OpiCa1-PEG-PLGA group after 12 h of intravenous injection (Mean ± SD, n = 6). Statistical significance was calculated using the two-tailed non-parametric Mann-Whitney T test for two groups' comparison. *P < 0.05; **P < 0.01.

5. Conclusion

In this study, OpiCal-PEG-PLGA nanomicelles were successfully synthesized for cardiac Ca^{2+} overload induced by β-adrenergic receptor stress. Applying it to mice with sudden cardiac death induced by adrenaline and caffeine, the survival rate of mice is over 90 %. Because OpiCal-PEG-PLGA nanomicelles maintain the biological function of the calcin, which enabled OpiCal-PEG-PLGA nanomicelles to quickly bind with RyRs, further activating RyRs, and dissociating from RyRs, to increase Ca^{2+} release from sarcoplasmic reticulum and prevent Ca^{2+} overload. In addition, compared with OpiCal, the structure of OpiCal-PEG-PLGA nanomicelles are more stable within 72 h at 4 °C. Cytotoxicity and organ toxicity of OpiCal-PEG-PLGA nanomicelles are also much lower than that of OpiCal. All results demonstrate OpiCal-PEG-PLGA nanomicelles have the potential to antagonize the sudden cardiac death in mice induced by epinephrine and caffeine and improve the prognosis of cardiac disease events. This study importantly provides theoretical and experimental basis for developing novel peptide nanomedicines to cure related diseases of sarcoplasmic reticulum Ca^{2+} overload.

Credit authors statement

Conceptualization: L.X., H.H.V., J.W.; Methodology: J.L., F.W., X.L.,; Investigation: J.L., F.W., Z.Y., H.Z., S.G., C.R.V.; Visualization: J.L., X.H., X.L., H.Z., S.G., C.R.V.; Supervision: L.X., H.H.V., J.W., J.L,. Y.H., Z.X., L. X., S.G.; Writing—original draft: J.L., F.W., X.L.; Writing—review & editing: J.L., F.W., Z.Y., H.Z., S.G., C.R.V., L.X., H.H.V., J.W.

Funding

This work was supported by the National Key R&D Program of China (2019YFE0116800), the China National Natural Science Foundation (Grant No.31972751), Shanxi Modern Agro-industry Technology Research System (2023) Shanxi Agricultural University Horizontal Science and Technology Project (Gtant No. 2022HX286)

Declaration of competing interest

The authors declare that they have no known competing financial interests or personal relationships that could have appeared to influence the work reported in this paper.

Data availability

Data will be made available on request.

Acknowledgments

We thank the Naval Medical University for Department of pharmacy for access to equipment and the department of Occupational and Environmental Health for resources that supported this study.We also thank the University of Wisconsin-Madison School of Medicine and Public Health for guide work.

Appendix A. Supplementary data

Supplementary data to this article can be found online at https://doi.org/10.1016/j.mtbio.2023.100859.

References

[1] A. Mahmood, K. Ahmed, Y. Zhang, β-Adrenergic receptor desensitization/down-regulation in heart failure: a friend or foe? Front Cardiovasc Med 9 (2022), 925692 https://doi.org/10.3389/fcvm.2022.925692.
[2] W. Peng, et al., Structural basis for the gating mechanism of the type 2 ryanodine receptor RyR2, Science 354 (2016), https://doi.org/10.1126/science.aah5324.
[3] X.H. Wehrens, Leaky ryanodine receptors cause delayed afterdepolarizations and ventricular arrhythmias, Eur. Heart J. 28 (2007) 1054–1056, https://doi.org/10.1093/eurheartj/ehm068.
[4] K. Demydenko, H.L. Roderick, The cardiomyocyte firestarter-RyR clusters ignite their neighbours after augmentation of Ca(2+) release by β-stimulation, Acta Physiol. 234 (2022), e13798, https://doi.org/10.1111/apha.13798.
[5] W. Wongcharoen, et al., Effects of a Na+/Ca2+ exchanger inhibitor on pulmonary vein electrical activity and ouabain-induced arrhythmogenicity, Cardiovasc. Res. 70 (2006) 497–508, https://doi.org/10.1016/j.cardiores.2006.02.026.
[6] N. Voigt, et al., Enhanced sarcoplasmic reticulum Ca2+ leak and increased Na+-Ca2+ exchanger function underlie delayed afterdepolarizations in patients with chronic atrial fibrillation, Circulation 125 (2012) 2059–2070, https://doi.org/10.1161/circulationaha.111.067306.
[7] S. Magi, V. Lariccia, M. Maiolino, S. Amoroso, S. Gratteri, Sudden cardiac death: focus on the genetics of channelopathies and cardiomyopathies, J. Biomed. Sci. 24 (2017) 56, https://doi.org/10.1186/s12929-017-0364-6.
[8] A. Garcia-Elias, B. Benito, Ion Channel disorders and sudden cardiac death, Int. J. Mol. Sci. 19 (2018), https://doi.org/10.3390/ijms19030692.
[9] A.T.H. Selnø, V.V. Sumbayev, B.F. Gibbs, IgE-dependent human basophil responses are inversely associated with the sarcoplasmic reticulum Ca(2+)-ATPase (SERCA), Front. Immunol. 13 (2022), 1052290, https://doi.org/10.3389/fimmu.2022.1052290.
[10] H.H. Valdivia, M.S. Kirby, W.J. Lederer, R. Coronado, Scorpion toxins targeted against the sarcoplasmic reticulum Ca(2+)-release channel of skeletal and cardiac muscle, Proc. Natl. Acad. Sci. U.S.A. 89 (1992) 12185–12189, https://doi.org/10.1073/pnas.89.24.12185.
[11] G.B. Gurrola, E.M. Capes, F.Z. Zamudio, L.D. Possani, H.H. Valdivia, Imperatoxin A, a cell-penetrating peptide from scorpion venom, as a probe of Ca-release channels/ryanodine receptors, Pharmaceuticals 3 (2010) 1093–1107, https://doi.org/10.3390/ph3041093.
[12] I.R. Seo, M.R. Choi, C.S. Park, D.H. Kim, Effects of recombinant imperatoxin A (IpTxa) mutants on the rabbit ryanodine receptor, Mol. Cell. 22 (2006) 328–335.
[13] M. Aureliano, et al., Inhibition of SERCA and PMCA Ca(2+)-ATPase activities by polyoxotungstates, J. Inorg. Biochem. 236 (2022), 111952, https://doi.org/10.1016/j.jinorgbio.2022.111952.
[14] A. Harguindey, et al., Synthesis and assembly of click-nucleic-acid-containing PEG-PLGA nanoparticles for DNA delivery, Adv. Mater. 29 (2017), https://doi.org/10.1002/adma.201700743.
[15] S. Pascual-Gil, T. Simón-Yarza, E. Garbayo, F. Prosper, M.J. Blanco-Prieto, Tracking the in vivo release of bioactive NRG from PLGA and PEG-PLGA microparticles in infarcted hearts, J. Contr. Release 220 (2015) 388–396, https://doi.org/10.1016/j.jconrel.2015.10.058.
[16] L. Xiao, et al., Structure-function relationships of peptides forming the calcin family of ryanodine receptor ligands, J. Gen. Physiol. 147 (2016) 375–394, https://doi.org/10.1085/jgp.201511499.
[17] E.F. Schwartz, et al., Characterization of hadrucalcin, a peptide from Hadrurus gertschi scorpion venom with pharmacological activity on ryanodine receptors, Br. J. Pharmacol. 157 (2009) 392–403, https://doi.org/10.1111/j.1476-5381.2009.00147.x.
[18] P. Lemieux, et al., Block and graft copolymers and NanoGel copolymer networks for DNA delivery into cell, J. Drug Target. 8 (2000) 91–105, https://doi.org/10.3109/10611860008996855.
[19] S. Ordanini, F. Cellesi, Complex polymeric architectures self-assembling in unimolecular micelles: preparation, characterization and drug nanoencapsulation, Pharmaceutics 10 (2018), https://doi.org/10.3390/pharmaceutics10040209.
[20] M. Yokoyama, Polymeric micelles as drug carriers: their lights and shadows, J. Drug Target. 22 (2014) 576–583, https://doi.org/10.3109/1061186x.2014.934688.
[21] D.N. Kapoor, et al., PLGA: a unique polymer for drug delivery, Ther. Deliv. 6 (2015) 41–58, https://doi.org/10.4155/tde.14.91.
[22] Y. Su, et al., PLGA-based biodegradable microspheres in drug delivery: recent advances in research and application, Drug Deliv. 28 (2021) 1397–1418, https://doi.org/10.1080/10717544.2021.1938756.
[23] A. Shariati, Z. Chegini, E. Ghaznavi-Rad, E.N. Zare, S.M. Hosseini, PLGA-based nanoplatforms in drug delivery for inhibition and destruction of microbial biofilm, Front. Cell. Infect. Microbiol. 12 (2022), 926363, https://doi.org/10.3389/fcimb.2022.926363.
[24] K. Zhang, et al., PEG-PLGA copolymers: their structure and structure-influenced drug delivery applications, J. Contr. Release 183 (2014) 77–86, https://doi.org/10.1016/j.jconrel.2014.03.026.
[25] F.M. Veronese, G. Pasut, PEGylation, successful approach to drug delivery, Drug Discov. Today 10 (2005) 1451–1458, https://doi.org/10.1016/s1359-6446(05)03575-0.
[26] D. Ding, Q. Zhu, Recent advances of PLGA micro/nanoparticles for the delivery of biomacromolecular therapeutics, Mater. Sci. Eng., C 92 (2018) 1041–1060, https://doi.org/10.1016/j.msec.2017.12.036.
[27] C.V. Rocha, V. Gonçalves, M.C. da Silva, M. Bañobre-López, Gallo, J. PLGA-based composites for various biomedical applications, Int. J. Mol. Sci. 23 (2022), https://doi.org/10.3390/ijms23042034.
[28] R. Mahar, et al., Application of PLGA as a biodegradable and biocompatible polymer for pulmonary delivery of drugs, AAPS PharmSciTech. 24 (2023) 39, https://doi.org/10.1208/s12249-023-02502-1.
[29] Y. Guo, et al., A light-controllable specific drug delivery nanoplatform for targeted bimodal imaging-guided photothermal/chemo synergistic cancer therapy, Acta Biomater. 80 (2018) 308–326, https://doi.org/10.1016/j.actbio.2018.09.024.

[30] K.M. Manto, et al., (4-Aminopyridine)-PLGA-PEG as a novel thermosensitive and locally injectable treatment for acute peripheral nerve injury, ACS Appl. Bio Mater. 4 (2021) 4140–4151, https://doi.org/10.1021/acsabm.0c01566.
[31] A.J. Lomant, G. Fairbanks, Chemical probes of extended biological structures: synthesis and properties of the cleavable protein cross-linking reagent [35S] dithiobis(succinimidyl propionate), J. Mol. Biol. 104 (1976) 243–261, https://doi.org/10.1016/0022-2836(76)90011-5.
[32] J.V. Staros, R.W. Wright, D.M. Swingle, Enhancement by N-hydroxysulfosuccinimide of water-soluble carbodiimide-mediated coupling reactions, Anal. Biochem. 156 (1986) 220–222, https://doi.org/10.1016/0003-2697(86)90176-4.
[33] Z. Grabarek, J. Gergely, Zero-length crosslinking procedure with the use of active esters, Anal. Biochem. 185 (1990) 131–135, https://doi.org/10.1016/0003-2697(90)90267-d.
[34] W. Wang, et al., Impact of particle size and pH on protein corona formation of solid lipid nanoparticles: a proof-of-concept study, Acta Pharm. Sin. B 11 (2021) 1030–1046, https://doi.org/10.1016/j.apsb.2020.10.023.
[35] T. Mueller, G. Ceder, Effect of particle size on hydrogen release from sodium alanate nanoparticles, ACS Nano 4 (2010) 5647–5656, https://doi.org/10.1021/nn101224j.
[36] L. Peltonen, Practical guidelines for the characterization and quality control of pure drug nanoparticles and nano-cocrystals in the pharmaceutical industry, Adv. Drug Deliv. Rev. 131 (2018) 101–115, https://doi.org/10.1016/j.addr.2018.06.009.
[37] V. Dave, et al., Lipid-polymer hybrid nanoparticles: development & statistical optimization of norfloxacin for topical drug delivery system, Bioact. Mater. 2 (2017) 269–280, https://doi.org/10.1016/j.bioactmat.2017.07.002.
[38] J.J. Carbó, et al., Carbon-nitrogen bond construction and carbon-oxygen double bond cleavage on a molecular titanium oxonitride: a combined experimental and computational study, Inorg. Chem. 54 (2015) 9401–9412, https://doi.org/10.1021/acs.inorgchem.5b00943.
[39] V. Mozhaeva, et al., Differentiation of snake venom using Raman spectroscopic analysis, J. Mater. Chem. B 11 (2023) 6435–6442, https://doi.org/10.1039/d3tb00829k.
[40] S. Choi, S.Y. Chun, K. Kwak, M. Cho, Micro-Raman spectroscopic analysis of liquid-liquid phase separation, Phys. Chem. Chem. Phys. 25 (2023) 9051–9060, https://doi.org/10.1039/d2cp05115j.
[41] I. Smirnov, Z. Kaszkur, A. Hoell, Development of nanoparticle bulk morphology analysis: a multidomain XRD approach, Nanoscale 15 (2023) 8633–8642, https://doi.org/10.1039/d3nr00456b.
[42] J.M. Gardin, F.M. Siri, R.N. Kitsis, J.G. Edwards, L.A. Leinwand, Echocardiographic assessment of left ventricular mass and systolic function in mice, Circ. Res. 76 (1995) 907–914, https://doi.org/10.1161/01.res.76.5.907.
[43] M. Scherrer-Crosbie, B. Kurtz, Ventricular remodeling and function: insights using murine echocardiography, J. Mol. Cell. Cardiol. 48 (2010) 512–517, https://doi.org/10.1016/j.yjmcc.2009.07.004.
[44] T. Suma, et al., Modulated fragmentation of proapoptotic peptide nanoparticles regulates cytotoxicity, J. Am. Chem. Soc. 139 (2017) 4009–4018, https://doi.org/10.1021/jacs.6b11302.
[45] X. Bai, et al., Regulation of cell uptake and cytotoxicity by nanoparticle core under the controlled shape, size, and surface chemistries, ACS Nano 14 (2020) 289–302, https://doi.org/10.1021/acsnano.9b04407.
[46] J. Tang, Y. Wu, S. Esquivel-Elizondo, S.J. Sørensen, B.E. Rittmann, How microbial aggregates protect against nanoparticle toxicity, Trends Biotechnol. 36 (2018) 1171–1182, https://doi.org/10.1016/j.tibtech.2018.06.009.
[47] Y. Marcus, N. Tal, M. Ronen, R. Carmieli, M. Gurevitz, The drug ornidazole inhibits photosynthesis in a different mechanism described for protozoa and anaerobic bacteria, Biochem. J. 473 (2016) 4413–4426, https://doi.org/10.1042/bcj20160433.
[48] L. Vargas-Jaimes, et al., Recombinant expression of Intrepicalcin from the scorpion Vaejovis intrepidus and its effect on skeletal ryanodine receptors, Biochim. Biophys. Acta Gen. Subj. 1861 (2017) 936–946, https://doi.org/10.1016/j.bbagen.2017.01.032.
[49] O. Haji-Ghassemi, et al., Cryo-EM analysis of scorpion toxin binding to Ryanodine Receptors reveals subconductance that is abolished by PKA phosphorylation, Sci. Adv. 9 (2023), eadf4936, https://doi.org/10.1126/sciadv.adf4936.
[50] D. Greene, M. Barton, T. Luchko, Y. Shiferaw, Molecular dynamics simulations of the cardiac ryanodine receptor type 2 (RyR2) gating mechanism, J. Phys. Chem. B 126 (2022) 9790–9809, https://doi.org/10.1021/acs.jpcb.2c03031.
[51] M.B. Cannell, C.H. Kong, M.S. Imtiaz, D.R. Laver, Control of sarcoplasmic reticulum Ca2+ release by stochastic RyR gating within a 3D model of the cardiac dyad and importance of induction decay for CICR termination, Biophys. J. 104 (2013) 2149–2159, https://doi.org/10.1016/j.bpj.2013.03.058.
[52] H. Cheng, S.Q. Wang, Calcium signaling between sarcolemmal calcium channels and ryanodine receptors in heart cells, Front. Biosci. 7 (2002) d1867–d1878, https://doi.org/10.2741/a885.
[53] J. Mustroph, et al., SR Ca(2+)-leak and disordered excitation-contraction coupling as the basis for arrhythmogenic and negative inotropic effects of acute ethanol exposure, J. Mol. Cell. Cardiol. 116 (2018) 81–90, https://doi.org/10.1016/j.yjmcc.2018.02.002.
[54] S.T. Ohnishi, et al., Abnormal membrane properties of the sarcoplasmic reticulum of pigs susceptible to malignant hyperthermia: modes of action of halothane, caffeine, dantrolene, and two other drugs, Arch. Biochem. Biophys. 247 (1986) 294–301, https://doi.org/10.1016/0003-9861(86)90587-4.
[55] A.F. Dulhunty, M.G. Casarotto, N.A. Beard, The ryanodine receptor: a pivotal Ca2+ regulatory protein and potential therapeutic drug target, Curr. Drug Targets 12 (2011) 709–723, https://doi.org/10.2174/138945011795378595.
[56] K. Xiong, et al., Enhanced bovine serum albumin absorption on the N-hydroxysuccinimide activated graphene oxide and its corresponding cell affinity, Mater. Sci. Eng., C 81 (2017) 386–392, https://doi.org/10.1016/j.msec.2017.08.044.
[57] B. Wang, J.S. Tian, Z.C. Zhou, [Food web in jellyfish-shrimp-shellfish polyculture pond], Ying yong sheng tai xue bao, J. Appl. Ecol. 32 (2021) 2028–2034, https://doi.org/10.13287/j.1001-9332.202106.009.
[58] H.F. Jiao, et al., Self-assembly of all-conjugated block copolymer nanoparticles with tailoring size and fluorescence for live cell imaging, J. Mater. Chem. B 4 (2016) 7882–7887, https://doi.org/10.1039/c6tb02211a.
[59] S. Shahriyar, S. Taymouri, S. Saberi, P. Asadi, M. Tabbakhian, Preparation and characterization of itraconazole loaded nanomicelles based on dextran-behenic acid for cutaneous leishmaniasis treatment, Drug Dev. Ind. Pharm. 47 (2021) 416–428, https://doi.org/10.1080/03639045.2021.1890112.
[60] E. Zdrali, Y. Chen, H.I. Okur, D.M. Wilkins, S. Roke, The molecular mechanism of nanodroplet stability, ACS Nano 11 (2017) 12111–12120, https://doi.org/10.1021/acsnano.7b05100.
[61] S. Lewis, New model jellyfish? Nat. Rev. Neurosci. 23 (2022) 69, https://doi.org/10.1038/s41583-021-00551-8.
[62] K. Liu, et al., The nanomicelles consisting of lotus root amylopectin and quinoa protein: construction and encapsulation for quercetin, Food Chem. 387 (2022), 132924, https://doi.org/10.1016/j.foodchem.2022.132924.
[63] R. Prakash, et al., NLRP3 inflammasome-targeting nanomicelles for preventing ischemia-reperfusion-induced inflammatory injury, ACS Nano 17 (2023) 8680–8693, https://doi.org/10.1021/acsnano.3c01760.
[64] X. Du, et al., Comprehensive evaluation of lipid nanoparticles and polyplex nanomicelles. For muscle-targeted mRNA delivery, Pharmaceutics 15 (2023), https://doi.org/10.3390/pharmaceutics15092291.
[65] M. Zhao, et al., Nucleic acid nanoassembly-enhanced RNA therapeutics and diagnosis, Acta Pharm. Sin. B 13 (2023) 916–941, https://doi.org/10.1016/j.apsb.2022.10.019.